Final report on neutron irradiation at low temperature to investigate plastic instability and at high temperature to study caviation

Singh, B.N; Eldrup, Morten Mostgaard; Golubov, D.J.; Edwards, D.J.; Jung, P.

Publication date:
2005

Document Version
Publisher's PDF, also known as Version of record

RISØ

Risø-R-1496(EN)

Final Report on Neutron Irradiation at Low Temperature to Investigate Plastic Instability and at High Temperature to Study Cavitation

B. N. Singh, M. Eldrup, S.I. Golubov, D.J. Edwards and P. Jung

Risø National Laboratory
Roskilde
Denmark
January 2005

Authors: B. N. Singh[1)], M. Eldrup[1)], S.I. Golubov[2)], D.J. Edwards[3)] and P. Jung[4)]

Report title: Final Report on Neutron Irradiation at Low Temperature to Investigate Plastic Instability and at High Temperature to Study Cavitation

[1)]Materials Research Department, Risø National Laboratory, DK-4000 Roskilde, Denmark
[2)]Metals and Ceramics Division, Oak Ridge National Laboratory, P.O. Box 2008, Oak Ridge, TN 37831-6376
[3)]Materials Structure and Performance Group, Pacific Northwest National Laboratory, Richland, WA 99352, USA
[4)]Forschungszentrum Jülich, IFF, Postfach 1913, D-52425 Jülich, Germany

Risø-R-1496(EN)
January 2005

ISSN 0106-2840
ISBN 87-550-3400-4 (Internet)

Abstract

Effects of neutron irradiation on defect accumulation and physical and mechanical properties of pure iron and F82H and EUROFER 97 ferritic-martensitic steels have been investigated. Tensile specimens were neutron irradiated to a dose level of 0,23 dpa at 333 and 573 K. Electrical resistivity and tensile properties were measured both in the unirradiated and irradiated condition. Some additional specimens of pure iron were irradiated at 333 K to doses of 10^{-3}, 10^{-2} and 10^{-1} dpa and tensile tested at 333 K. To investigate the effect of helium on cavity nucleation and growth, specimens of pure iron and EUROFER 97 were implanted with different amounts of helium at 323 K and subsequently neutron irradiated to doses of 10^{-3}, 10^{-2} and 10^{-1} dpa at 323 K. Defect microstructures were investigated using positron annihilation spectroscopy (PAS) and transmission electron microscopy (TEM). Numerical calculations, based on the production bias model (PBM) were carried out to study the details of evolution of cavities with and without helium generation. The phenomena of dislocation decoration and raft formation, which are important for understanding radiation hardening and plastic flow localization, have been studied using the Kinetic Monte Carlo (KMC) code during a realistic dynamic irradiation of bcc iron at 300 K. Molecular dynamics (MD) simulations have been carried out to study the stress dependencies of dislocation velocity and drag coefficient for an edge dislocation decorated with small SIA loops.The present report describes both experimental procedure and calculational methodology employed in the present work. The main results of all these investigations, both experimental and theoretical, are highlighted with appropriate examples. Finally, a brief summary is given of the main results conclusions.

Contract no.: TW2-TTMS001-Del 08 (EFDA)

Group's own reg. no.: 1610008-00

Sponsorship:
EU-Fusion Technology Programme

Cover :

Pages: 38
Tables: 4
References: 34

Risø National Laboratory
Information Service Department
P.O.Box 49
DK-4000 Roskilde
Denmark
Telephone +45 46774004
bibl@risoe.dk
Fax +45 46774013
www.risoe.dk

Contents

1 Introduction

Effects of neutron irradiation on defect accumulation and its impacts on physical and mechanical properties of the reduced activation ferritic-martensitic (RAFM) steels are being extensively studied internationally since these are considered to be candidate materials for the blanket and the first wall of fusion reactor (e.g. DEMO and Commercial) [1]. These alloys are considered to have a number of more attractive properties than alternative structural materials such as austenitic stainless steels or vanadium alloys [2].

Although the ferritic-martensitic class of steels are resistant to void swelling and maintain good fracture toughness at irradiation temperatures above 673 K [3], they are prone to loss of ductility at lower irradiation temperatures [4, 5]. Furthermore, we have demonstrated recently that in pure iron as well as F82H steel neutron irradiation causes void formation already at temperatures as low as 323 - 373 K [6-8]. This is in agreement with general experimental observations that voids in bcc metals and alloys are formed at relatively low temperatures (i.e. close to the recovery stage III (see [9] for a review). Recent theoretical calculations have shown that the void nucleation at low temperatures in bcc crystals can be understood in terms of clustering of self-interstitial atoms (SIAs) in displacement cascades generated by fission or fusion neutrons and the mobility of these clusters. The scale of nucleation is found to be controlled by the diffusivity of vacancies and/or gas atoms [10].

The fact that these alloys will be exposed to 14 MeV neutrons in a fusion reactor introduces yet another complication due to concurrent generation of displacement cascades and helium atoms at a relatively high rate. Although it is well known that the presence of helium enhances the nucleation of voids (see Singh and Trinkaus [11] for a review), the mechanisms controlling the scale of nucleation and the level of resulting swelling are still not well understood.

The present work was initiated to investigate various aspects of damage accumulation and its impact on deformation behaviour (e.g. loss of ductility) at low temperatures (i.e. below the recovery stage V) and the role of helium on void formation at higher temperatures (i.e. above the recovery stage V) both experimentally and theoretically. The experimental investigations were designed to support and validate the basis and the main conclusions of analytical and numerical calculations. It should be mentioned that since the complexity of the microstructure of the ferritic-martensitic steels does not render them suitable for mechanistic studies, the theoretical investigations have been focused so far on pure bcc iron. In the following, the main results of both experimental and theoretical investigations are briefly summarized.

2 Materials and Experimental Procedure

For mechanical testing, tensile specimens of pure (99.9999%) iron were fabricated from a thin (0.25 mm) sheet. After fabrication tensile specimens were annealed at 923 K for 2 h in vacuum. Tensile specimens of F82H and EUROFER 97 reduced activation steels were fabricated from the common European stock available at PSI (Switzerland) in the as-tempered condition. The specimens of pure iron were irradiated in the as-annealed condition whereas the specimens of F82H and EUROFER 97 steels were irradiated in the as-tempered condition. Irradiations were carried out in the BR-2 reactor at Mol (Belgium) at 333 and 573 K to a dose level of ~0.23 dpa.

In another series of experiments, 100 μm thick sheets of pure iron and EUROFER 97 were manufactured from the same stock as described in [8]. Strip

specimens (20 x 3 x 0.1 mm^3) and dog-bone shaped 20 mm long tensile specimens (with gauge length and width of 8 and 3 mm, respectively) of both pure iron and EUROFER 97 steel were implanted with helium at Forschungszentrum Jülich (Germany). A beam of 28 Mev α-particles, energy degraded by a rotating wheel equipped with Al foils, was used for implantation of the specimens to provide a homogeneous He concentration throughout a depth of about 100 μm. The implantations were carried out at 323 K to doses of 1, 10 and 100 appm of helium at a rate of 2 x 10^{-2} appm He/s. On average, each implanted He atom gives rise to 155 atomic displacements. Hence, during the implantation, the displacement damage rate was ~3.1 x 10^{-6} dpa/s. Both unimplanted and He-implanted specimens were irradiated with fission neutrons in the BR-2 reactor at Mol (Belgium) at 323 K with a displacement dose rate of ~4.5 x 10^{-8} dpa/s to doses of 10^{-3}, 10^{-2} and 10^{-1} dpa. For comparison purposes, some unimplanted tensile specimens of the standard thickness (~250 μm) were also irradiated at 323 K to doses of 10^{-3}, 10^{-2} and 10^{-1} dpa.

Both unirradiated and irradiated specimens of pure iron, F82H and EUROFER 97 reduced activation steels were tensile tested at irradiation temperature at a strain rate of 1.3 x 10^{-3} s^{-1} in a vacuum of 10^{-2} Pa.

For transmission electron microscopy (TEM) investigations, 1 mm wide and ~0.1 mm thick strips were prepared from the irradiated materials. Thin foils were obtained from these strips by electropolishing at 20V in a solution of 20% perchloric acid in methanol at the ambient temperature. The thin foils were examined in a 200 keV JEOL 2000 FX electron microscope.

For each positron annihilation spectroscopy (PAS) investigation, two samples of approximately 5 × 3 mm^2 were cut from one strip specimen. The samples were cleaned by electropolishing prior to the measurements. A conventional positron lifetime spectrometer was used. For most of the He implanted specimens, measurements were carried out with both the beam entry side and the "back" side of the samples facing the positron source.

The electrical conductivity measurements were made on the unirradiated and irradiated tensile specimens and were carried out as described in [12].

3 Results

3.1 Electrical resistivity measurements

The specimens used for electrical conductivity measurements were the same as those used for tensile measurements or 3mm wide strips. Specimen thickness was ~100 μm or ~300 μm.

All conductivity measurements were carried out at room temperature, using a PC controlled unit developed at Risø National Laboratory. The unit applies a four-point technique and switches the current direction to eliminate the influence of thermo-voltage on the resulting conductance. All measurements were carried out with two different units to assure reproducibility. An overall systematic uncertainty on the measured conductances, mainly due to uncertainties on the effective sample dimensions, was estimated to be about ± 2%. For each set of measurements, the conductivity, σ_0, of one or more reference samples (Fe or EUROFER 97) was measured. For simplicity and in order to reduce possible systematic errors, the results for neutron irradiated and He implanted specimens are presented as relative values, i.e. normalised to the relevant reference sample conductivity (σ/σ_0).

Measurements were carried out for neutron irradiated Fe, and F82H as well as for He implanted Fe and EUROFER 97.

The conductivities for neutron irradiated Fe, EUROFER 97 and F82H (Table 1) were measured several times on the same specimens. The numbers given in the table are averages of these results and the quoted uncertainties are derived from the scatter. The result for irradiated Fe is in agreement with results obtained in [7].

Table 1. Electrical conductivity of Fe, F82H and EUROFER 97, neutron irradiated at 60°C to a displacement damage dose of 0.23 dpa. Relative resistivities (and conductivities) for the irradiated specimens are obtained by normalising their resistivities to the resistivity values for un-irradiated Fe and EUROFER 97, respectively.

	Resistivity (μΩcm)	Relative Resistivity	Relative Conductivity (%)
Fe reference	10.17 ± 0.2	1	100
Fe irradiated	11.6 ± 0.2	1.14 ± 0.02	87.7 ± 2
EUROFER 97 reference	41.2 ± 0.5	1	100
EUROFER 97 irradiated	45.2 ± 0.5	1.10 ± 0.02	91.2 ± 2
F82H irradiated	45.0 ± 0.5	1.09 ± 0.02	91.6 ± 2

For the He implanted specimens (Table 2) measurements were carried out on several nominally identical samples and the conductivity values given in the table obtained as averages of these results. The quoted uncertainties were derived from the scatter of the data. The large uncertainties for the specimens implanted at 50 °C are due to scatter between the different samples.

Table 2. Electrical conductivity of Fe and EUROFER 97, helium implanted at 50°C and 350°C. Relative resistivities (and conductivities) for the implanted specimens are obtained by normalising their resistivities to the resistivity values for un-irradiated Fe and EUROFER 97, respectively.

	Implantation temp. (°C)	He dose (appm)	Resistivity (μΩcm)	Relative Resistivity	Relative Conductivity (%)
Fe reference			10.19 ± 0.20		
Fe	50	100	11.14 ± 0.59	1.093 ± 0.06	91.5 ± 6
Fe	350	10	10.16 ± 0.08	0.997 ± 0.008	100.3 ± 0.8
Fe	350	100	10.29 ± 0.05	1.010 ± 0.005	99.0 ± 0.5
EUROFER reference			41.2 ± 0.5		
EUROFER 97	50	100	44.6 ± 4.0	1.083 ± 0.10	92.3 ± 10
EUROFER 97	350	10	42.5 ± 0.2	1.032 ± 0.006	96.9 ± 0.6
EUROFER 97	350	100	41.9 ± 0.9	1.017 ± 0.02	98.3 ± 2

3.2 Positron annihilation spectroscopy (PAS)

Positron annihilation spectroscopy (PAS) has in recent years been accepted as a very useful method for defect spectroscopy, in particular in studies of metals and semiconductors. The physical basis for this is the fact that positrons injected into a material may get trapped at defects that represent regions where the atomic density is lower than the average density in the bulk, i.e vacancies, vacancy clusters (including voids and bubbles) and dislocations. Since positrons and electrons are antiparticles, an injected positron will annihilate with an electron of the material. As a result, γ-rays will be emitted, which carry information about the state of the positron before annihilation, and by proper measurement of the emitted γ-quanta it is possible to obtain useful information about those defects that have trapped the positrons. This is in brief the physics behind PAS. A more detailed discussion and relevant references can be found in e.g. [13, 14].

In the present work the positron lifetime technique has been applied to measure the distributions of lifetimes of injected positrons, so-called positron lifetime spectra. Normally, regions of lower-than-average atomic density also have lower-than-average electron density. The lifetime of positrons trapped in defects will depend on the average electron density in the defects (the lower the electron density, the longer is the lifetime). So in principle, each type of defect gives rise to a characteristic positron lifetime, τ_i. In cases where several types of defects are present in a sample, a measured lifetime spectrum will therefore consists of several lifetime components. Each component is a decaying exponential, the slope of which equals the annihilation rate ($= \tau_i^{-1}$). Examples of positron lifetime spectra are shown in figures 1, 2, 4 and 5. The figures display both single- and multi-component spectra.

In bulk Fe the positron lifetime is 106 ps, while in defects such as mono-vacancies, dislocations, loops and SFTs the lifetimes are found to be in the range of ~120 - ~180 ps. The lifetime of positrons trapped in three-dimensional vacancy agglomerates (voids) increases with the size of the voids, the lifetime value thus being a measure of the void size, up to a saturation value of about 500 ps for voids containing more than ~ 40 - 50 vacancies. The presence of He (or other gases) in a cavity will reduce the lifetime.

In the following we shall briefly show PAS results obtained for iron and EUROFER 97 implanted at ~ 50°C with He to different dose levels and subsequently neutron irradiated. In order to illustrate directly the obtained positron lifetime data for implanted and irradiated iron and EUROFER 97 steel, we show some of the measured lifetime spectra.

Figure 1 clearly shows that in Fe, the average positron lifetime increases with increasing He dose. For comparison, spectra for neutron irradiated Fe [7] at about the same displacement damage doses are also shown. Generally, the average positron lifetime is somewhat shorter for the He implanted than for the neutron-irradiated iron. Fig. 2 compares the effect of neutron irradiation after He implantation with the effect of only neutron irradiation or only He implantation to about the same displacement dose level. In Fig. 3, which shows the mean positron lifetime as a function total displacement dose, the data from Figs. 1 and 2 are summarized. For both neutron irradiation [7] and He implantation the mean lifetime increases with dose, the latter lifetime being lower than the former in the whole dose range. This lowering of the positron lifetime in the He implanted specimens is at least partly due to the presence of He in the cavities created during implantation.

The purpose of the brief mean-positron-lifetime description in the above paragraph for some of the measured Fe specimens was to give a simple qualitative impression of the general trend of the results. Also a more detailed analysis of the measured lifetime spectra was carried out. All spectra could be decomposed into three lifetime components using the PATFIT programs [15]. The results are shown in Table 3.

Table 3. Positron lifetimes and intensities for He implanted and neutron irradiated Fe. The data are for the selected spectra shown in Figs. 1 and 2. The lifetimes τ_3 are due to 3-dimensional cavities that consist of 10 vacancies or more, while the lifetimes τ_2 are due to other defects, including vacancy "clusters" with ~ 1 - 5 vacancies.

He dose (appm)	Neutron dose (dpa)	τ_1 (ps)	τ_2 (ps)	τ_3 (ps)	I_1 (%)	I_2 (%)	I_3 (%)
0	0	106 ± 1	-	-	100	0	0
1	0	67± 7	153 ± 10	305 ± 10	33.0 ± 3.2	52.1 ± 1.8	14.9 ± 1.9
10	0	47 ± 5	184 ± 10	345 ± 10	23.1 ± 2.3	38.9 ± 6.4	38.0 ± 7.2
100	0	43 ± 15	198 ± 17	379 ± 12	12.3 ± 1.6	46.4 ± 1.4	41.4 ± 1.5
100	0.01	104 ± 7	256 ± 13	407 ± 10	14.8 ± 2.5	40.1 ± 0.5	45.1 ± 2.1
0	0.009	49 ± 6	280 ± 5	409 ± 11	7.2 ± 1.0	67.4 ± 4.4	25.4 ± 4.5

Like for neutron irradiated Fe [7] the lifetimes associated with vacancies and 3-dimensional vacancy agglomerates (sometimes referred to as nano-voids), i.e. τ_2 and τ_3 increase with dose, in the present case He dose. This indicates that the cavity sizes increase with increasing displacement damage dose. However, the values of the lifetimes are generally lower than the ones for neutron irradiated Fe, which – at least in part – must be ascribed to trapping of He in the defects.

Based on the data in Table 3 it is possible to make quantitative estimates of the sizes and densities of the cavities that give rise to the τ_3, I_3 lifetime component. Two extreme situations may be considered, one in which we assume that essentially all He has been trapped in the cavities, and one which assumes that the He is trapped in other defects than in the cavities. In the first case, we follow the scheme developed by Jensen et al. [16], which leads to estimates of bubble diameters of 0.8 nm and 2.4 nm with estimated densities of about 10^{23} m^{-3} and 3×10^{22} m^{-3} for implantation of 10 and 100 appm He, respectively. In the second case, the approach of [7] is used, which gives estimates for the diameters of 0.6 nm and 0.7 nm with densities of 2×10^{23} m^{-3} and 3×10^{23} m^{-3} for 10 and 100 appm He implantation, respectively. The results for 10 appm He implantation are not very different in the two cases, while for 100 appm He the two cases lead to appreciable size differences and ten times higher density if empty cavities are assumed. The first assumption (all He in the bubbles) leads to an estimated decrease in bubble density with increasing He dose as well as to a bubble size of about 2.4 nm in specimens implanted with 100 appm He. Such bubbles have not been observed by TEM (the other calculated sizes are too small to be observed by TEM). Hence, these two unexpected results of the estimate makes this assumption less credible. Therefore we are lead to the conclusion that the observed cavities do not contain all the implanted He and that the second assumption (and hence sizes and densities based on that) are more realistic. This is in agreement with results of annealing experiments on for example Cu [13] and Ni [17] which were He implanted at room temperature. These measurements suggested that the cavities, which were formed during implantation, decreased in size and/or received an influx of He atoms during annealing at about $0.4\times T_m$ (where T_m is the melting temperature) before they grew in size at higher annealing temperature. It would be interesting to carry out similar annealing experiments on the He implanted specimens. Such investigations are being planned.

Figure 4 shows positron lifetime spectra for EUROFER 97, which was implanted with 1, 10, and 100 appm of He at ~ 50°C as well as the spectrum for un-

implanted (i.e. as-tempered) EUROFER 97. This latter lifetime spectrum shows a somewhat longer average lifetime than for pure Fe (compare with Fig. 1 or 2). The quantitative analysis shows that a major fraction of the positrons have a lifetime of 145 ps, which means that they are trapped in a population of defects, present already before He implantation and neutron irradiation. This lifetime is close to the one found for as-tempered F82H steel [18] and it is reasonable to ascribe the lifetime to positrons trapped at dislocations. This defect population, maybe somewhat modified, is likely to be present also in the implanted and irradiated specimens and will make a quantitative analysis of the results for such specimens more uncertain than is the case for pure Fe.

The effect of He implantation of EUROFER 97, shown in Fig. 4, is smaller than for Fe (Fig. 1), and in contrast to the lifetime variation for Fe, the average lifetime increases for 1 and 10 appm He but decreases again for 100 appm. The reason for this unexpected variation is not yet clear. On the other hand, Fig. 5 demonstrates that neutron irradiation, with or without prior implantation of He, leads to a stronger lifetime increase, although not as strong as in the case of pure Fe (compare Fig. 2). Figure 6, which shows the mean positron lifetime as a function of total displacement dose, summarizes the data presented in Figs. 4 and 5. The small effect of He implantation in contrast to the effect of neutron irradiation is clearly displayed.

Like for Fe, a quantitative analysis of the lifetime data for EUROFER 97 was carried out. The results are shown in Table 4.

Table 4. Positron lifetimes and intensities for He implanted and neutron irradiated EUROFER 97. The data are for the selected spectra shown in Figs. 3 and 4. The lifetimes τ_3 are due to small 3-dimensional cavities of less than 15 vacancies, while the lifetimes τ_2 are due to other defects, for neutron irradiated specimens vacancy "clusters" consisting of a few vacancies.

He dose (appm)	Neutron dose (dpa)	τ_1 (ps)	τ_2 (ps)	τ_3 (ps)	I_1 (%)	I_2 (%)	I_3 (%)
0	0	63 ± 11	145 ± 2	-	14.1 ± 3.4	85.9 ± 3.4	0
1	0	80 ± 12	152	244 ± 11	10.2 ± 2.5	79.5 ± 4.6	10.3 ± 2.2
10	0	6 ± 17	152	255 ± 3	9.3 ± 5.8	69.1 ± 4.6	21.6 ± 1.4
100	0	68 ± 2	152	402 ± 25	22.3 ± 0.5	76.7 ± 0.7	1.0 ± 0.2
100	0.01	99 ± 15	207 ± 5	397 ± 20	17.1 ± 2.4	72.6 ± 1.9	10.3 ± 0.6
0	0.01	103 ± 12	217 ± 5	394 ± 20	13.0 ± 1.4	72.4 ± 0.8	14.6 ± 0.8

As mentioned above, the quantitative analysis of the lifetime spectra for EUROFER 97 is associated with larger uncertainties than is the case for Fe. However, the lifetime τ_2 for the specimens which are only He implanted is very close to the defect lifetime for the un-implanted sample and may therefore be associated with the same type of defect, probably dislocations. The $\tau_2 \sim 210$ ps after neutron irradiation may arise from clusters of only 2 – 3 vacancies or from bigger agglomerates which also contain He. Similarly the values of $\tau_3 \sim 250$ ps for He implantation of 1 and 10 appm may be associated with vacancy clusters of about 4 vacancies or bigger He bubbles. Lifetimes of $\tau_3 \sim 400$ ps (after neutron irradiation) are characteristic of nano-voids containing about 15 vacancies each, if we assume (as discussed above for the results for Fe) that these cavities contain only little He. We estimate the densities of these nano-voids in excess of 10^{23} m^{-3}.

In Figure 7 we show micrograph for pure Fe implanted with 100 appm He and subsequently neutron irradiated to a dose level of 0.1 dpa, both at about 50°C. A population of interstitial clusters with a density of about 4×10^{22} m^{-3} was observed, but in addition to this - quite unexpectedly - also a rather low density (~ 2×10^{19} m^{-3}) of relatively large voids were found. Such voids were not observed in the equivalent samples studied by PAS, but the low void density would make it very difficult to detect them in the presence of higher densities of other defects, which trap the positrons (see above). This surprising finding of large voids after low-temperature implantation and irradiation will be further investigated.

3.3 Tensile properties

Tensile specimens of pure iron (annealed at 923 K for 2 h in vacuum), F82H and EUROFER 97 steels were irradiated at 333 K and 573 K with fission neutrons in the BR-2 reactor at Mol (Belgium) to a dose level of ~0.23 dpa and were tested at 333 and 573 K. For comparison, the reference unirradiated specimens of pure iron, F82H and EUROFER 97 steel were also tensile tested at 333 and 573 K. Figures 8 and 9 show the engineering stress-strain curves for the specimens tested at 333 and 573 K, respectively, both in the unirradiated and irradiated conditions. The results show that the irradiation at 333 K even to this relatively low displacement damage level of only ~0.23 dpa, causes a significant decrease in the uniform elongation of both F82H and EUROFER 97 steels. Furthermore, after irradiation at 333 K both these steels loose the ability to work harden during post-irradiation deformation and exhibit a clear tendency of plastic instability. It should be noted that these steels do not provide any evidence of a yield drop during post-irradiation testing at 333 K. In contrast, the irradiation at 333 K does seem to induce a yield drop in the case of pure iron. However, after the initial yield drop, the iron specimen shows the tendency to workharden and yields the uniform elongation, which is very similar to that in the unirradiated condition (see Fig. 8a).

A comparison of the results shown in Figs. 8b and 9b reveals, on the other hand, that the irradiation at 573 K does not seem to have any significant effect either on the hardening (i.e. increase in the yield strength) or the uniform elongation. It is worth noting, however, that the uniform elongation of F82H and EUROFER 97 is lower at 573 K than at 333 K, both in the unirradiated and irradiated conditions.

Some additional specimens of pure and annealed (923 K, 2 h) iron were irradiated with fission neutrons in the BR-2 reactor at Mol (Belgium) at 333 K to displacement doses of 10^{-3}, 10^{-2} and 0.23 dpa. As usual, the tensile specimens were 0.25 mm thick. Both the unirradiated and irradiated specimens were tensile tested at 333 K with a strain rate of 1.3 x 10^{-3} s^{-1}. The engineering stress-strain curves are shown in Fig. 10. It can be seen that even though the unirradiated specimen does not show any sign of well defined yield drop, the occurrence of a yield drop is clearly seen in all the irradiated specimens. Furthermore, although the yield strength increases with increasing displacement dose level, the flow strength (i.e. beyond the yield point) first decreases and then increases with increasing the dose level.

4 Modelling Activities

Our modeling activities address some aspects of two major problems arising from the effects of neutron irradiation on (a) mechanical properties at relatively low irradiation temperatures (i.e. below the recovery stage V) and (b) helium transport and accumulation in metals and alloys both below and above the recovery stage V. It is well known, for instance, that neutron irradiation at low temperatures causes a significant amount of hardening and leads to yield drop, plastic instability and a

drastic decrease in the uniform elongation. This poses a serious problem for materials considered for their application in the structural components of a fusion reactor. Another problem arises due to production of helium and hydrogen at relatively high rates during irradiation with 14 MeV neutrons. At high temperatures the accumulation of helium at grain boundaries in the form of bubbles may lead to grain boundary embrittlement and may limit the lifetime of components such as the first wall and divertor. Furthermore, the continuous generation of helium may also affect the swelling and creep behaviour at relatively high temperatures. Unfortunately, none of these problems and the mechanisms controlling them are well understood.

In an effort to improve our understanding of the processes controlling the effect of irradiation on mechanical properties, some modelling activities were initiated already some years ago. Some of the results on iron have been reported in earlier publications (e.g. [19 – 22]). The modelling work in this area has continued. The computational methodology used and some of the results obtained will be summarised in the following sections. Recently, some modelling activities on effects of helium on cavity nucleation and growth have been initiated and some of the preliminary results are also described.

4.1 Production, segregation and accumulation of interstitial clusters during neutron irradiation

It is well known that during neutron irradiations at low temperatures (i.e. below the recovery stage V), the accumulation of interstitial clusters produced directly in the cascades occurs in a very segregated fashion. The segregation of interstitial loops in the forms of decoration of grown-in dislocations and rafts of loops is particularly prominent in bcc crystals since most of the interstitial clusters produced in the cascades are highly glissile. In view of these observations, it was proposed already in 1997 that the irradiation-induced increase in the upper yield stress and the occurrence of yield drop could be rationalized in terms of the so-called cascade induced source hardening (CISH) model [23]. The model assumes, however, that most of the grown-in dislocations get decorated by the glissile interstitial clusters produced in the cascades and thereby become unable to operate as dislocation sources. Later, it was shown by analytical calculations using the linear elasticity theory that such dislocation decoration can occur [24].

For further validation of this idea that the grown-in dislocations do indeed get decorated by SIA clusters (loops) produced directly in the cascades, Kinetic Monte Carlo (KMC) simulations have been carried out. These simulations are designed to study not only dislocation decoration and raft formation but also the accumulation of SIA clusters during a real dynamic irradiation experiment. In the present simulations, the defects generated by a number of 40 keV cascades corresponding to a damage rate of 5×10^{-8} dpa/s are introduced at the appropriate frequency in the simulation box ($0.25 \times 25 \times 0.25$ μm^3). Point defect statistics for clusters generated by 40 keV cascades in α-Fe (e.g. number, size distribution and mobility) are taken from the Molecular Dynamics (MD) simulations of Bacon et al. [25]. The magnitude of 1-D diffusional glide of the SIA clusters and the frequency of change in direction of these clusters are also taken from the results of MD simulations [e.g. 19].

As the density of defect clusters builds up with increasing displacement dose, their temporal and spatial evolution is followed by the KMC code. The present code incorporates the elastic interactions among the SIA clusters, between the SIA clusters and the grown-in dislocations and between the SIA clusters and the nano-voids. The mean size of the nano-voids is taken to be equivalent to cavities containing 100 vacancies. As cluster density increases with increasing dose level, the calculation of interactions amongst all the clusters becomes very time consuming.

Consequently, so far, the microstructural evolution has been calculated to doses of only up to 5.21 x 10^{-3} dpa (see [26] for details). The results of the KMC simulations with the above mentioned production and interaction conditions show that the density of SIA clusters (containing more than 4 SIAs) builds up very rapidly with increasing dose level. The dose dependence of the total cluster density is shown in Fig. 11. The results have been obtained for two different conditions: (i) when nano-voids are assumed to be absent and (ii) when the density of nano-voids is assumed to follow the experimental results of PAS measurements [7]. Clearly, the presence of a high density of nano-voids tends to induce a saturation in the cluster density already at a dose level of ~10^{-3} dpa. Figure 12 shows the dose dependence of the density of visible clusters of SIAs containing 100 or more SIAs. The results of TEM investigations of cluster density in pure iron irradiated with neutrons at 323 – 343 K [7, 27] are also shown in Fig. 12. It is encouraging to note that the general trend of the dose dependence of the cluster density obtained from present simulations is rather similar to that shown by the experimental results.

Figure 13 shows the evolution of dislocation decoration at (a) 1.3 x 10^{-3} dpa and (b) 5.2 x 10^{-3} dpa, indicating that the dislocation decoration begins to occur at rather low doses. Similar TEM results have been reported for neutron irradiated single crystal molybdenum [28]. However, it should be pointed out that no such observations have been reported for neutron irradiated iron. Figure 14 shows an example of segregation of SIA clusters in the form of a raft of loops at a dose level of 1.8 x 10^{-3} dpa. It should be mentioned that raft formation has been observed in neutron irradiated single crystal molybdenum at similar doses [28] but not in pure iron. In pure iron rafts of SIA loops have been observed after neutron irradiation but at a considerably higher dose level of 0.4 – 0.7 dpa [7, 8]. It could be that the presence of impurities in iron may be responsible for this delay since impurity atoms may alter the mobility of 1-D diffusing SIA clusters. This problem is currently being investigated and the results will be reported later.

4.2 Dynamic properties of dislocations decorated with interstitial loops

As discussed in the previous section (section 4.1) most of the SIA clusters produced in the cascades in iron during neutron irradiation are glissile and readily lead to dislocation decoration and formation of rafts of SIA loops. According to the cascade induced source hardening (CISH) model [23], it is expected that both of these occurrences would have significant effects on the deformation behaviour of irradiated materials. It should be recognized, however, that this expectation has its origin in calculations which are based on isotropic elasticity theory and assuming that the dislocation lines are static and rigid.

In real deformation experiments, on the other hand, dislocations would be mobile and flexible and would have physical (close distance) interaction with SIA clusters present in the glide plane of the dislocation. It has been shown earlier [8, 20], however, that the close-distance interactions between a dislocation line and SIA clusters (loops) cannot be calculated accurately using the linear isotropic elasticity theory. It is, therefore, of interest to investigate the dynamic properties of mobile undecorated dislocations as well as of dislocations decorated with small SIA clusters (loops) using atomic-scale simulation technique such as molecular dynamics (MD).

In the present work, the motion of undecorated and decorated dislocations at zero and non-zero (300 K) temperatures has been studied using molecular statics (MS) and molecular dynamics (MD) techniques, respectively. In both cases a model based on a periodic array of edge dislocations has been employed. Both bcc iron and fcc copper crystals contain about 750.000 atoms.

Simulations are carried out using many-body interatomic potentials derived by Ackland et al. [29, 30]. In the case of decorated dislocations, the Burgers vector of the SIA loops decorating the dislocation is taken to be the same as that of the moving edge dislocation. The spacing between the clusters is taken to be 11.2 nm. The interstitial clusters were of hexagonal shape and contained 37 SIAs both in iron and copper. The centre of the cluster was positioned at a distance of 11 lattice parameters below the slip plane containing the mobile dislocation. Details of the simulations and the results thereof are described in Ref. [31].

Using these simulations, first of all stress-strain relationship is obtained using a strain increment of 10^{-5}. This is followed by determination of the influence of the applied resolved shear stress on dislocation velocity for undecorated and decorated dislocations in bcc iron and fcc copper at 300 K (see Fig. 15). It can be seen in Fig. 15 that although the stress dependence of the velocity for iron and copper is very similar, the dislocation velocity at a given stress level is significantly lower in copper than that in iron. An interesting feature demonstrated by these simulations is that the moving dislocations drag the small SIA loops decorating them up to a certain stress level beyond which the moving dislocation breaks away from the loops. The breakaway stress levels in iron and copper are indicated in Fig. 15 by vertical arrows. This happens because the resistive force to cluster motion arising from drag also increases with increasing stress level and at a certain stress level becomes higher than the dislocation-cluster (loop) interaction force.

From the results shown in Fig.15, the stress dependence of the drag coefficient defined as $B = \tau b/v$ (where τ is the applied shear stress, b the magnitude of Burgers vector and v the dislocation velocity) is obtained and is plotted in Fig. 16 for both undecorated and decorated dislocations at the simulation temperature of 300 K. Clearly, the drag coefficient in copper particularly at lower stresses is considerably higher and the breakaway stress is considerably lower than that in iron. These differences seem to arise due partly to the higher effective drag coefficient in copper and partly the smaller maximum force a loop experiences in these materials.

Finally, it should be emphasized that the results of the present simulations, showing that under the influence of applied stress a moving edge dislocation decorated with SIA clusters can drag these clusters at high speed, cannot be described within the framework of continuum mechanics. The results also indicate that the atomic structure of dislocations and SIA clusters affects significantly the drag process. This effect cannot be easily treated in terms of the linear elasticity theory. These dynamic effects may have significant impacts on the evolution of dislocation microstructure and mechanical response of material exposed to irradiation conditions where dislocations and SIA clusters (in displacement cascades) would be produced concurrently and continuously (e.g. in-reactor deformation experiments).

4.3 Evolution of cavities with and without helium generation

The problem of void swelling at elevated temperatures is a matter of concern for structural materials employed particularly in the environment of 14 MeV neutrons in a fusion reactor. The concern arises from the fact that the 14 MeV neutrons not only produce displacement cascades but they also generate helium atoms via nuclear reaction at a relatively high rate. The kinetics of defect accumulation under these conditions is very complicated and is not well understood, particularly in bcc crystal structure. Further complications arise from the fact that in bcc crystals cavities are formed already at temperatures as low as 323 K and at the dose level as low as 10^{-4} dpa [7,8]. To our knowledge, there exists no theoretical framework at present within which the details of cavity nucleation can be adequately treated particularly for the condition of concurrent generation of cascades and helium atoms. It is well known,

however, that the creation of an excess of vacancies (i.e. vacancy supersaturation) during irradiation and the concentration of the available gas atoms are two most potent parameters that control the scale of cavity nucleation at a given irradiation temperature. Analytical calculations of vacancy supersaturation and its dose and temperature dependencies [10] have illustrated at least qualitatively that under the cascade damage condition, the effective vacancy supersaturation is dominated by the production bias [10].

The present work has been initiated to perform detailed numerical calculations of temporal evolution of vacancy concentration and supersaturation and kinetics of cavity nucleation and growth under cascade damage conditions. The computer code developed earlier to treat the problem of void swelling within the framework of the production bias model (PBM) has been modified to include the treatment of concurrent generation of helium and displacement cascades. In order to investigate the effect of helium on the evolution of cavity microstructure under cascade damage condition, it was necessary to find the solution of two-dimensional kinetic equation for the size distribution function of helium-vacancy clusters in pure iron implanted with helium or irradiated with neutrons. In order to reduce the number of equations needed to be solved for describing the evolution of helium-vacancy complexes, a new grouping method has been employed to integrate the kinetic equations.

While calculating the impact of helium atoms on cavity nucleation particularly under the condition of concurrent production of displacement cascades and mutational helium atoms two further complications arise. The first problem arises from the fact that the diffusion mechanism of helium atoms under these conditions still remains uncertain (see e.g. [11, 32, 33]. On the other hand, the diffusivity of helium plays a vital role in determining the scale of cavity nucleation [32-34]. The second problem arises from the fact that small cavities may perform Brownian-like motion. The coalescence of these small, mobile cavities may reduce the final density of cavities (e.g. see [32]). For these reasons computer code for the numerical calculation of cavity density during helium implantation as well as during neutron irradiation after helium implantation are being revised. These modifications, on the other hand, are not necessary for calculating the evolution of single defects produced during (a) neutron irradiation and (b) helium implantation at 323 K. These calculations have been performed within the framework of the PBM. The preliminary results for the cases of neutron irradiation as well as helium implantation are shown in Fig. 17 for pure iron. As indicated on the figures, the calculations are carried out for the damage parameters appropriate for the neutron irradiation and the helium implantation.

It can be seen in Fig. 17 that the dose dependences of the concentration of vacancies, SIAs and SIA clusters in pure iron during neutron irradiation is significantly different from those obtained during helium implantation. In the case of neutron irradiation the vacancy concentration reaches a maximum at a dose level of $\sim 10^{-4}$ dpa whereas in the case of helium implantation the vacancy concentration does not reach its maximum level even at the highest dose level. During helium implantation the buildup of SIA clusters continues up to about 10^{-4} dpa whereas during the neutron irradiation the concentration of SIA clusters saturates already at a dose level of about 10^{-7} dpa and at a much lower level than that during helium implantations. These differences seem to arise because of the differences in the damage production efficiency and efficiency of in-cascade clustering of SIAs between the neutron irradiation and helium implantation.

5 Summary and Conclusions

The main objective of the present report is to provide appropriate documentations for the investigations carried out with the aim of studying various aspects of damage accumulation during neutron irradiation and its impact on the physical and mechanical properties of pure iron and ferritic-martensitic steels. This has been already done in the previous sections. Presently, we shall present a brief summary of the main results described in the earlier sections.

The evolution of the irradiation-induced defect microstructure was characterized in detail using PAS, TEM and electrical conductivity measurements. The corresponding effects of defect accumulation on mechanical properties were characterized by uniaxial tensile testing.

Electrical conductivity measurements were carried out at room temperature on iron, F82H and EUROFER 97 steels neutron irradiated to a dose level of 0.23 dpa at 333 K and on Fe and EUROFER 97 implanted at 323 K and 623 K to doses of 10 and 100 appm He. The steels have an electrical conductivity, which is about four times lower than that for iron, but neutron irradiation decreases the relative conductivities by roughly the same amount, i.e. for Fe by about 12% and for the steels by about 9%. Implantation of Fe at 323 K with 100 appm He reduces the conductivity by about 8%, while no reduction can be detected on implantation at 623 K. For EUROFER 97 the uncertainty on the conductivity results prevents any quantitative statements about the magnitude of the reduction in conductivity caused by He implantation.

The positron annihilation spectroscopy investigations of He implantation of Fe and EUROFER 97 at 323 K revealed a clear difference between the two materials. The positron lifetimes in Fe increased with He dose in the range 1 – 100 appm, although the increase was not as strong as for neutron irradiation to the same displacement damage dose levels. This lifetime increase is due primarily to the formation of nano-voids and it is argued that an appreciable fraction of the implanted He does not get trapped in these small cavities. For He doses of 10 – 100 appm cavity sizes and densities were estimated to be 0.6 – 0.7 nm and 2 - 3×10^{23} m^{-3}. In case of neutron irradiation, implantation of He before the irradiation showed only a minor influence on the creation of nano-voids.

Helium implantation of EUROFER 97 leads to much smaller changes of positron lifetimes than observed for iron, and 100 appm He actually reduces the lifetime compared to 10 appm. This effect requires further investigation. Neutron irradiation, on the other hand, gives a stronger lifetime increase (with or without prior He implantation) although not as strong as in the case of pure Fe. The recorded positron lifetimes for He implanted EUROFER 97 can be ascribed to small vacancy clusters containing up to about five vacancies, increasing to about 15 vacancies after neutron irradiation.

Experimental results have shown that the neutron irradiation of F82H and EUROFER 97 steels at 333 K to a dose level of only 0.23 dpa causes loss of ductility, loss of work hardening ability and seems to induce even plastic instability. Pure iron, on the other hand, behaves very differently in that although it suffers from yield drop, it work hardens reasonably well and exhibits reasonable amount of uniform elongation.

The dose dependence of the deformation behaviour of pure iron irradiated at 333 K and tensile tested at 333 K illustrates two interesting features. First, although the yield strength increases with increasing dose level, the flow strength (i.e. beyond the yield point) first decreases and then increases with increasing dose level. Second, the magnitude of the yield drop increases with increasing dose level. These features are important from the point of view of modelling the deformation behaviour of pure iron during dynamic irradiation conditions (e.g. in-reactor tensile test).

The experimental results of post-irradiation tests show that the irradiation of pure iron as well as F82H and EUROFER 97 steels at 573 K does not have any significant effect on hardening and ductility.

The general tendency of the dose dependence of the increase in the density of SIA clusters obtained using the present KMC is reasonably consistent with experimental results reported for neutron irradiated pure iron. Note that the presence of nano-voids slows down the build-up of SIA clusters and seems to cause almost a saturation of the cluster density already at a dose level of less than 10^{-2} dpa. The present simulations also show that the decoration of dislocations by SIA loops and the formation of rafts of loops can easily occur in pure iron during neutron irradiation. This is also consistent with experimental observations.

Using the molecular dynamics simulation technique the stress dependencies of the dislocation velocity and the drag coefficient have been evaluated for both undecorated dislocations and dislocations decorated with SIA loops. Both kinds of dislocations are likely to be mobile during a dynamic deformation experiment. An interesting feature demonstrated by these simulations is that the moving dislocations drag the small SIA loops decorating them up to a certain stress level beyond which the moving dislocation breaks away from the loops. This means that during an in-reactor deformation experiment, the moving dislocation containing loop decoration will collect even more loops formed on the dislocation glide plane and will get even more strongly decorated. As a result, the long-range transport of dislocations will be seriously restricted which is likely to lead to a microstructure with a high density of very slowly moving dislocations. This problem in being further investigated.

In order to evaluate the role of helium in cavity nucleation and growth during 14 MeV neutron irradiation in a fusion reactor, preparations have been made to perform detailed numerical calculations within the framework of the PBM. Calculations will be carried out at low (below the recovery stage V) and at high temperatures (above the recovery stage V). As a first step, we have calculated the evolution of defect concentrations as a function of displacement dose level for the cases of neutron irradiation as well as helium implantation. Both sets of calculations have been carried out for an irradiation temperature of 323 K. The dose evolution of the vacancy and interstitial concentrations in the case of neutron irradiation is very different from those in the case of helium implantation. These differences seem to arise because of the differences in the damage production efficiency and the efficiency of in-cascade clustering of SIAs between the neutron irradiation and helium implantation.

Acknowledgements

The work reported here was partly funded by the European Fusion Technology Programme. The authors would like to thank Dr. Patrice Jacquet for Organizing irradiations in BR-2 reactor at Mol (Belgium).

References

1 R.L. Klueh, K. Ehrlich and F. Abe, J. Nucl. Mater. 191 – 194 (1992) 116.
2 K. Ehrlich and K. Anderko, J. Nucl. Mater. 171 (1990) 139.
3 D.S. Gelles, J. Nucl. Mater. 212 – 215 (1994) 714; 233 – 237 (1996) 293.
4 J.M. Vitek, W.R. Corwin, R.L. Klueh and J.R. Hawthorne, J. Nucl. Mater. 141 – 143 (1986) 948.
5 V.S. Khabarov, A.M. Dvoriashin and S.I. Porolle, J. Nucl. Mater. 233 – 237 (1996) 236.
6 M. Eldrup and B.N. Singh, J. Nucl. Mater. 276 (2000) 269.
7 M. Eldrup, B.N. Singh, S.J. Zinkle, T.S. Byun and K. Farrel, J. Nucl. Mater. 307 – 311 (2002) 912.
8 B.N. Singh, Risø Report No. Risø-R-1422(EN), August 2003, p. 28.
9 B.N. Singh and J.H. Evans, J. Nucl. Mater. 226 (1995) 29.
10 H. Trinkaus and B.N. Singh, J. Nucl. Mater. 307 – 311 (2002) 900.
11 B.N. Singh and H. Trinkaus, J. Nucl. Mater. 186 (1992) 153.
12 M. Eldrup and B.N. Singh, J. Nucl. Mater. 258 – 263 (1998) 1022.
13 M. Eldrup and B.N. Singh, J. Nucl. Mater. 251 (1997) 132.
14 M. Eldrup, J. Phys. (Paris) IV Colloq. 5 (1995) C1-93.
15 P. Kirkegaard, N.J. Pedersen and M. Eldrup, PATFIT-88, Risø-M-2740, Risø National Laboratory (1989).
16 K.O. Jensen, M. Eldrup, B.N. Singh and M. Victoria, J. Phys. F 18 (1988) 1069.
17 D. Segers I. Lemahieu, L. Deschepper, M. Dorikens, D. Geshef, L. Dorikens-Vanpraet, L.M. Stals, G. Severne and A. Hermanne, p. 416, in Proceedings of 8'th International Conference on Positron Annihilation (eds: L. Dorikens-Vanpraet, M. Dorikens and D. Segers). World Scientific (1989).
18 M. Eldrup and B.N. Singh, Risø Report No. Risø-R-1241 (EN), December 2001.
19 Yu. N. Osetsky, D.J. Bacon, A. Serra, B.N. Singh and S.I. Golubov, J. Nucl. Mater. 276 (2000) 65.
20 Yu. N. Osetsky, D.J. Bacon, A. Serra and B.N. Singh, MRS Symp. Proc. 653 (2001) Z3.4.
21 B.N. Singh, N.M. Ghoniem and H. Trinkaus, J. Nucl. Mater. 307 – 311 (2002) 159.
22 N.M. Ghoniem, S.H. Tong, J. Huang, B.N. Singh and M. Wen, J. Nucl. Mater. 307 – 311 (2002) 843.
23 B.N. Singh, A.J.E. Foreman and H. Trinkaus, J. Nucl. Mater. 249 (1997) 103.
24 H. Trinkaus, B.N. Singh and A.J.E. Foreman, J. Nucl. Mater. 251 (1997) 172.
25 D.J. Bacon, F. Gao and Yu. N. Osetsky, J. Nucl. Mater. 276 (2000) 1.
26 M. Wen, N.M. Ghoniem and B.N. Singh, Phil. Mag. (2005), in press.
27 B.N. Singh, A. Horsewell and P. Toft, J. Nucl. Mater. 271 – 272 (1999) 97.
28 B.N. Singh, J.H. Evans, A. Horsewell, P. Toft and G.V. Müller, J. Nucl. Mater. 258 – 263 (1998) 865.
29 G.J. Ackland, G. Tichy, V. Vitek and M.V. Finnis, Phil. Mag. A56 (1987) 735.
30 G.J. Ackland, D.J. Bacon, A.F. Calder and T. Harry, Phil. Mag. A75 (1997) 713.
31 Yu. N. Osetsky, D.J. Bacon, Z. rong and B.N. Singh, Phil. Mag. Letters (2005), in press.

32 A.J.E. Foreman and B.N. Singh, J. Nucl. Mater. 141 – 143 (1986) 672.
33 H. Trinkaus, B.N. Singh and A.J.E. Foreman, J. Nucl. Mater. 174 (1990) 80.
34 A.J.E. Foreman and B.N. Singh, Radiation Effects and Defects in Solid, 113 (1990) 175.

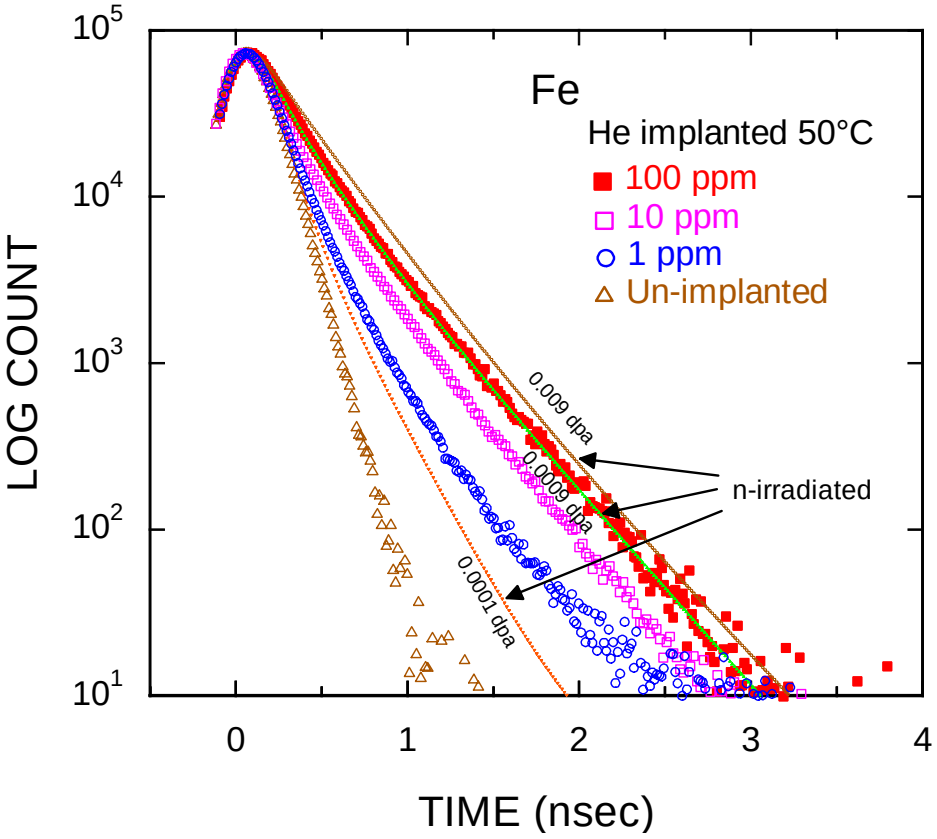

Figure 1. Positron lifetime spectra for Fe, which has been implanted with 1, 10, and 100 appm of He at ~ 50°C. The increase of the average positron lifetime reflects the formation of He bubbles and other microstructural defects. The spectra for He implantation are compared with spectra for neutron irradiated Fe. The spectra are similar, but for comparable displacement damage doses, spectra for He implantation are somewhat below those for neutron irradiation (implantation with 1, 10 and 100 appm He leads to displacement damage doses of 1.5×10^{-4}, 1.5×10^{-3}, and 1.5×10^{-2} dpa, respectively).

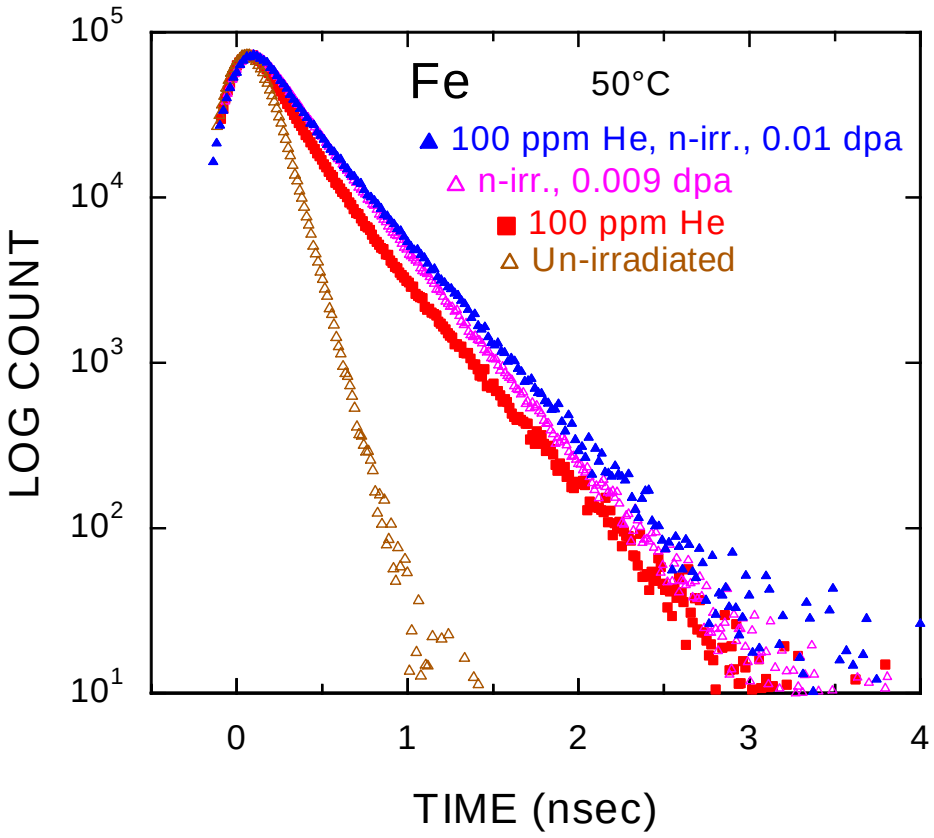

Figure 2. Comparison of positron lifetime spectra for Fe, which has either been implanted with 100 appm He, neutron irradiated to a displacement dose of 0.009 dpa or neutron irradiated (0.009 dpa) after He implantation (100 appm).

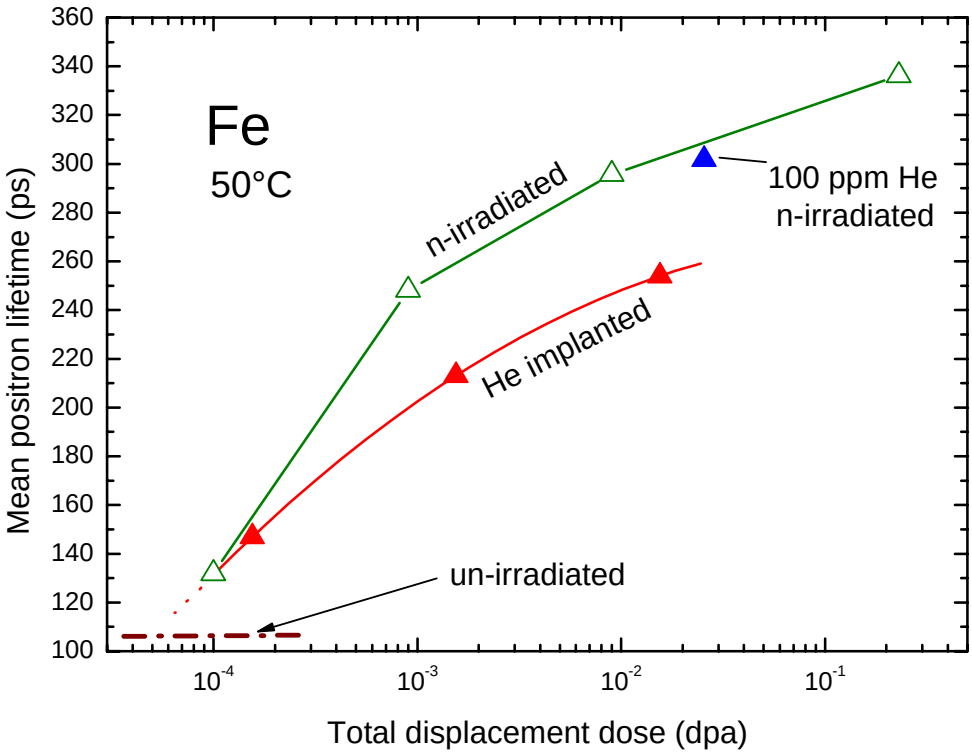

Figure 3. Mean positron lifetimes calculated from the spectra shown in Figs. 1 and 2 as functions of total displacement dose. The green curve for neutron irradiated specimens is based on data from [7].

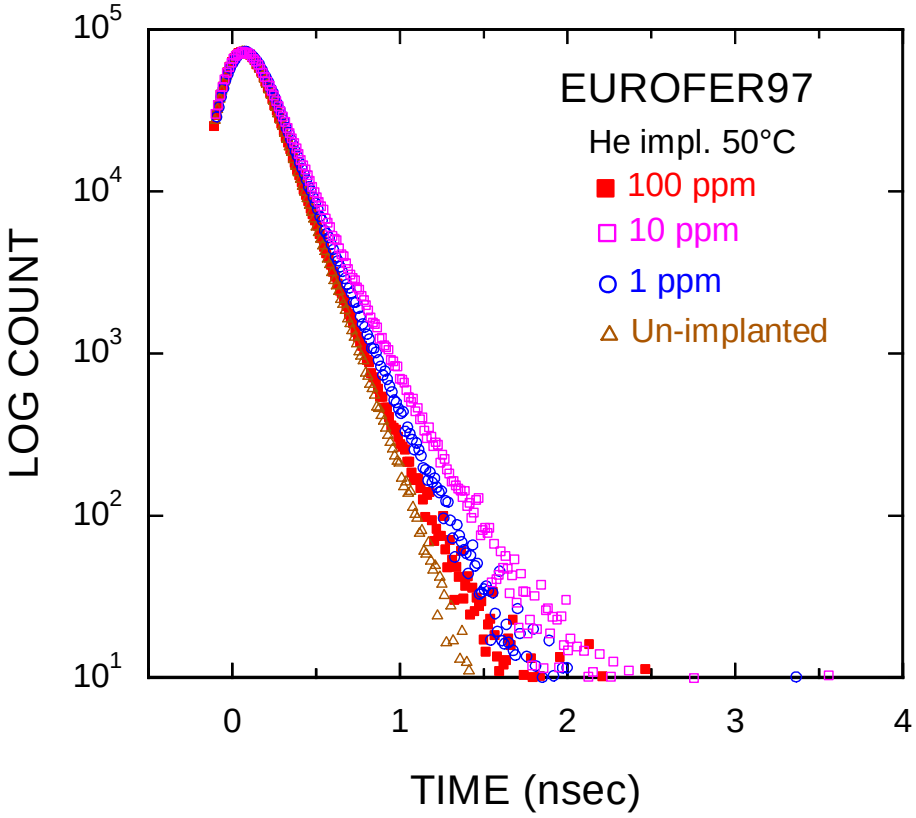

Figure 4. Positron lifetime spectra for EUROFER 97, which has been implanted with 1, 10, and 100 appm of He at ~ 50°C. Clearly, the effect of implantation is smaller than for Fe (Fig. 1), and in contrast to the lifetime variation for Fe, the average lifetime increases for 1 and 10 appm He but decreases again for 100 appm.

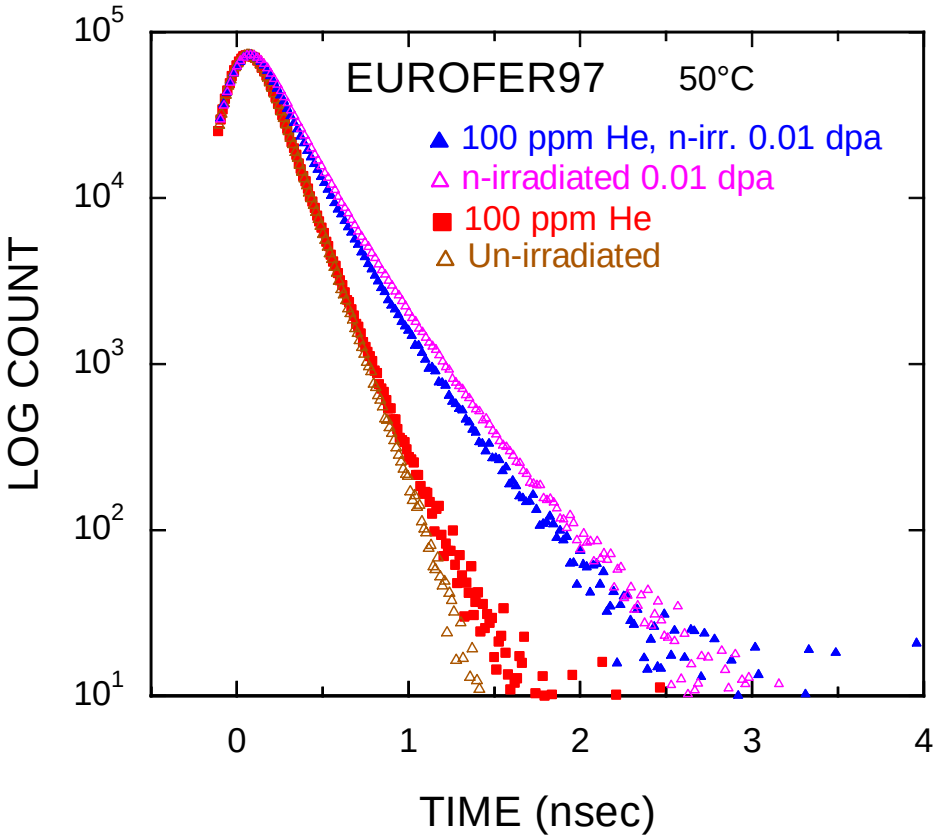

Figure 5. Comparison of positron lifetime spectra for EUROFER 97, which has either been implanted with 100 appm He, neutron irradiated to a displacement dose of 0.01 dpa or neutron irradiated (0.01 dpa) after He implantation (100 appm). The effect of neutron irradiation (with or without prior He implantation) is much stronger than that of He implantation alone, but smaller than for Fe (Fig. 2).

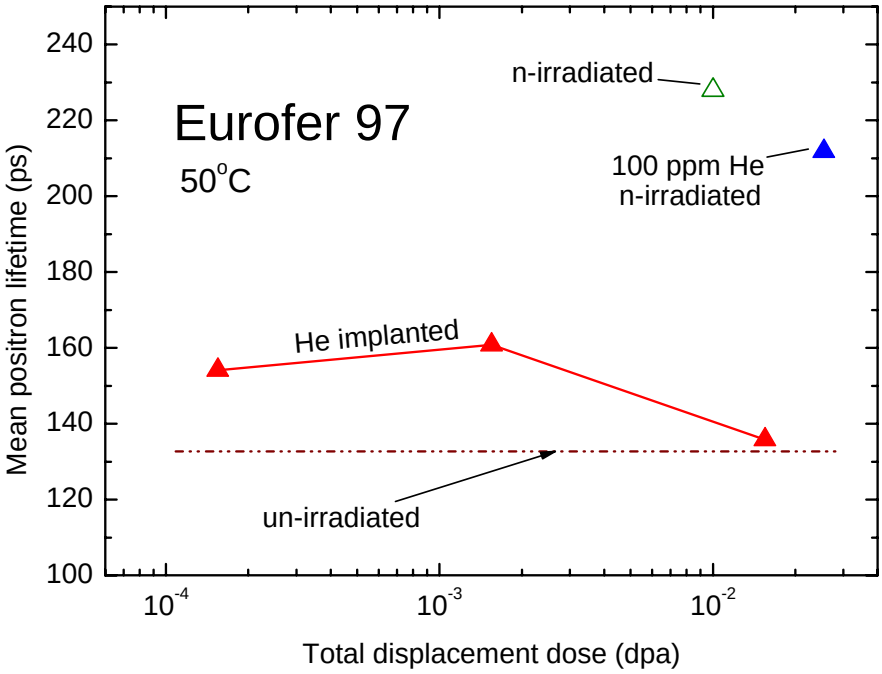

Figure 6. Mean positron lifetimes calculated from the spectra shown in Figs. 4 and 5 as functions of total displacement dose.

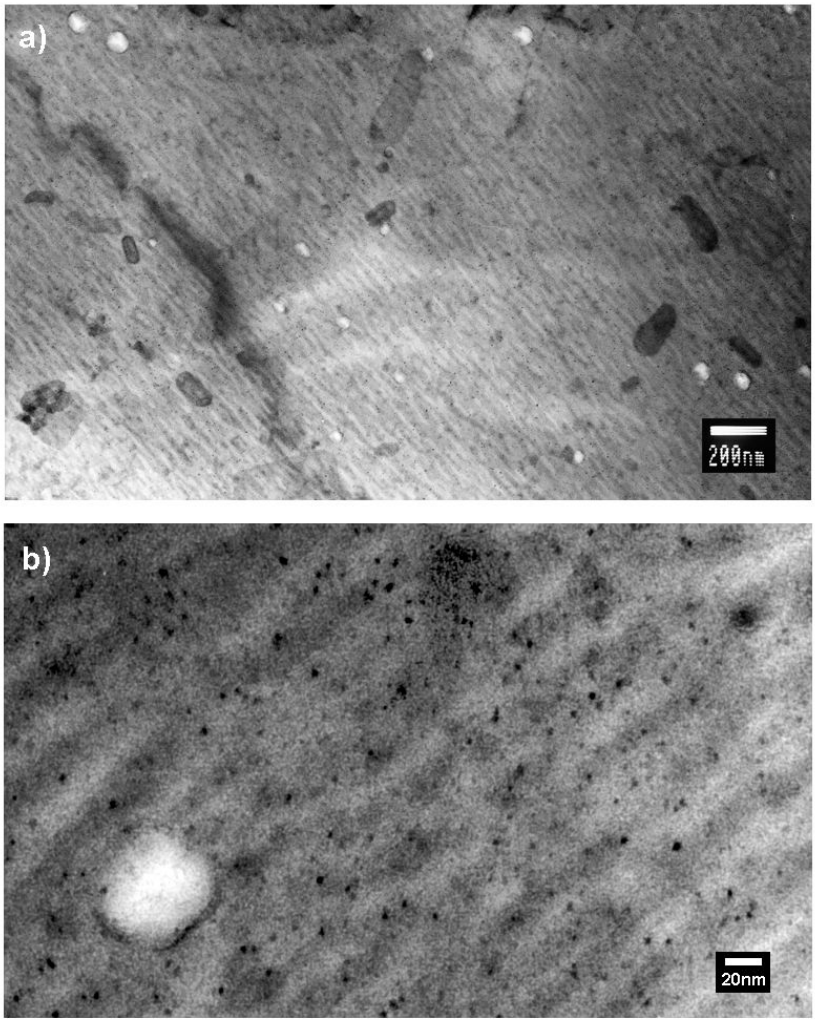

Figure 7. Transmission electron micrograph for pure iron implanted with 100 appm of helium at 323 K and subsequently neutron irradiated at 333 K to a dose level of 0.1 dpa showing: (a) relatively large voids (~52 nm in diameter) and (b) small (~4 nm in diameter) interstitial clusters. The density of voids and loops is estimated to be 2×10^{19} m^{-3} and $\sim 4 \times 10^{22}$ m^{-3}, respectively.

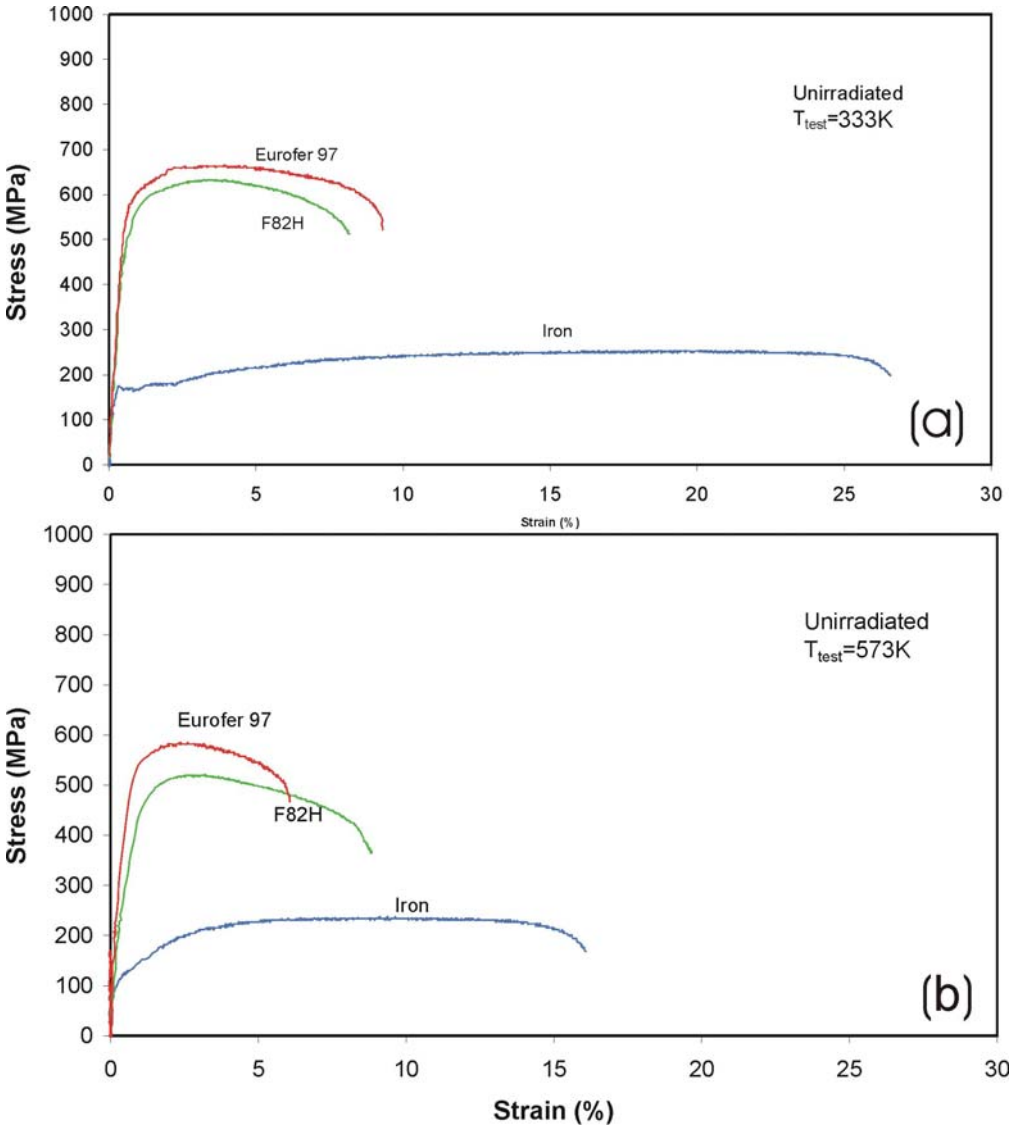

Figure 8. Stress-strain curves for pure iron, F82H and EUROFER 97 steels tested in the unirradiated condition at (a) 333 K and (b) 573 K.

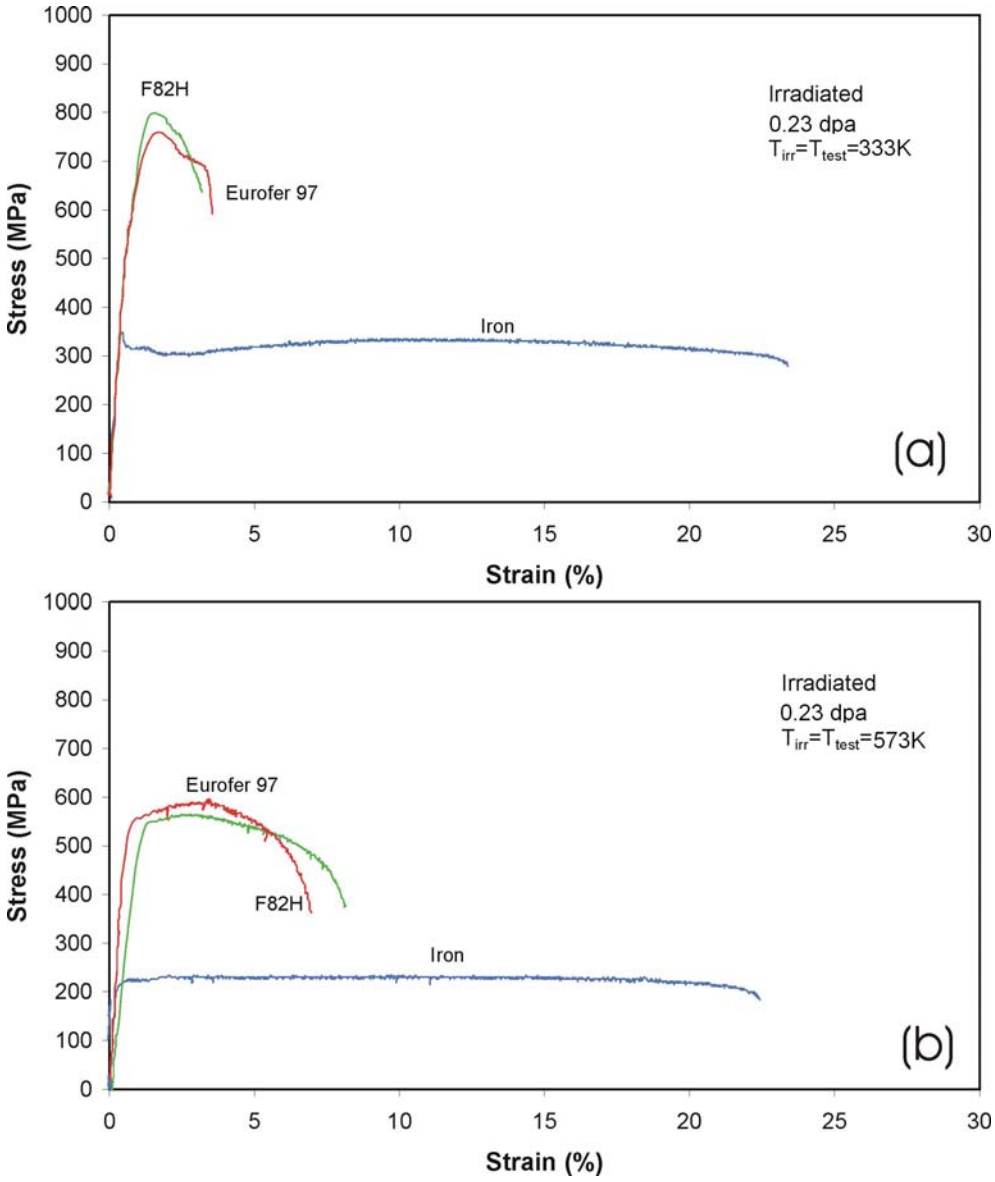

Figure 9. Same as Figure 8 but tested after neutron irradiation at (a) 333 K and (b) 573 K to a dose level of 0.23 dpa.

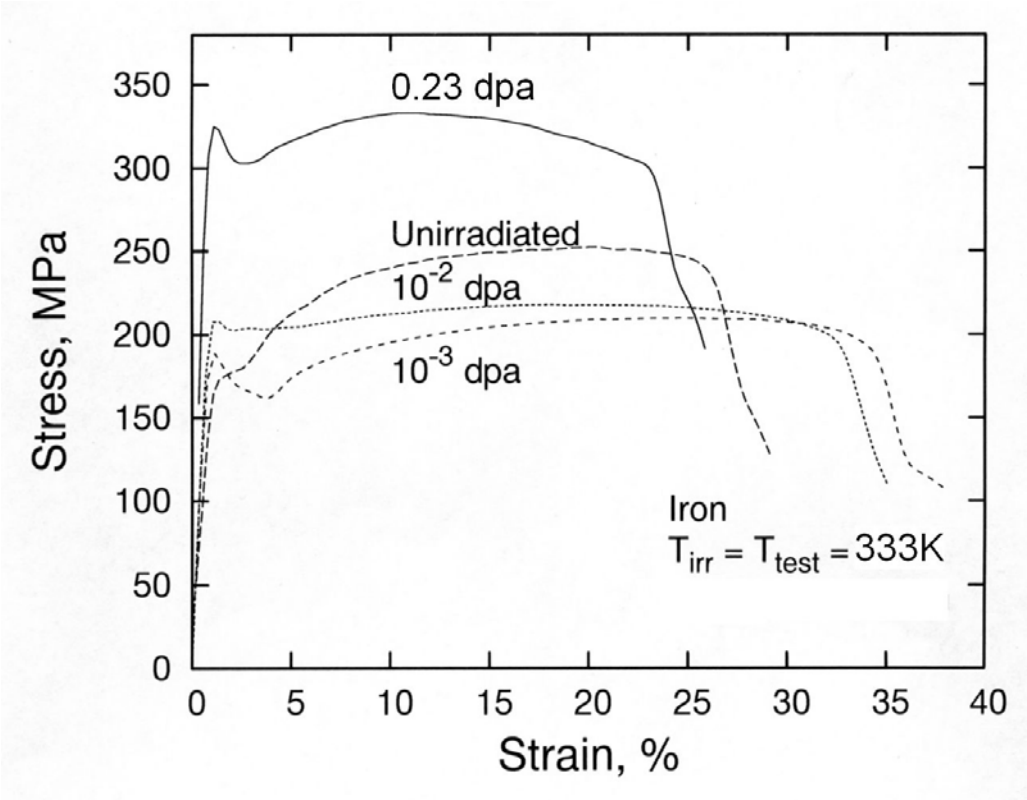

Figure 10. Stress-strain curves for pure iron neutron irradiated at 333 K to doses of 0.001, 0.01 and 0.23 dpa. For comparison, the stress-strain curve for the unirradiated pure iron tested at 333 K is also shown. Note that although the yield stress increases with the irradiation dose, the flow stress first decreases after irradiation to 0.001 and 0.01 dpa and then increases at a dose level of 0.23 dpa.

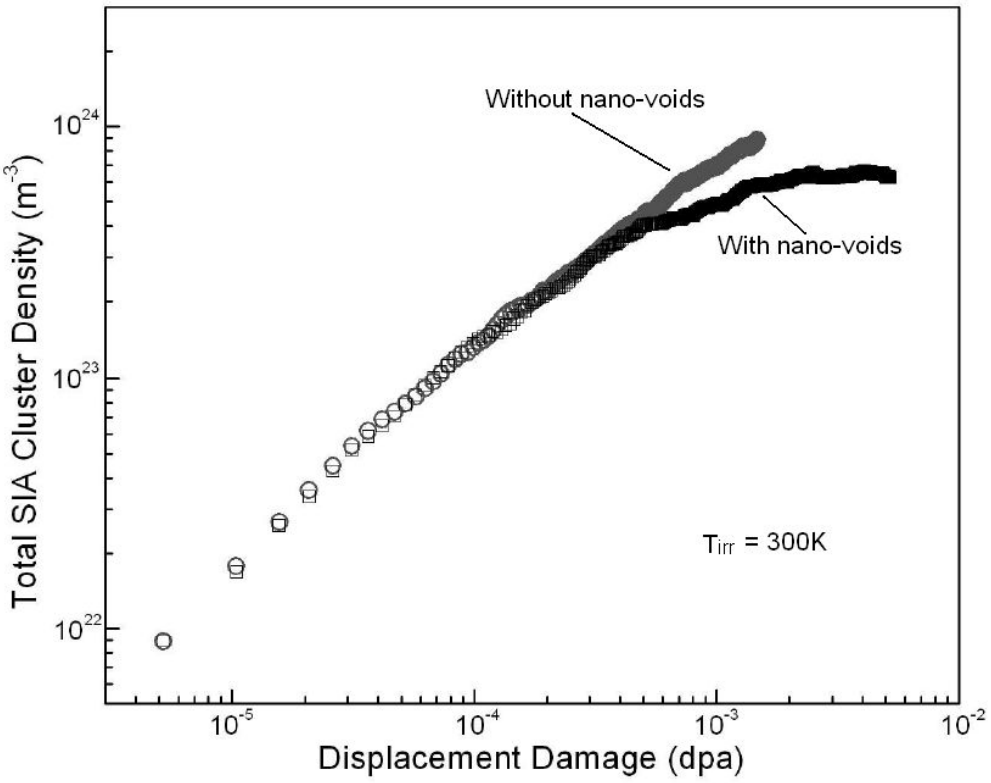

Figure 11. Dose dependence of the total density of SIA clusters calculated for pure bcc iron corresponding to neutron irradiation at 300 K (□) with and (0) without the presence of nano-voids.

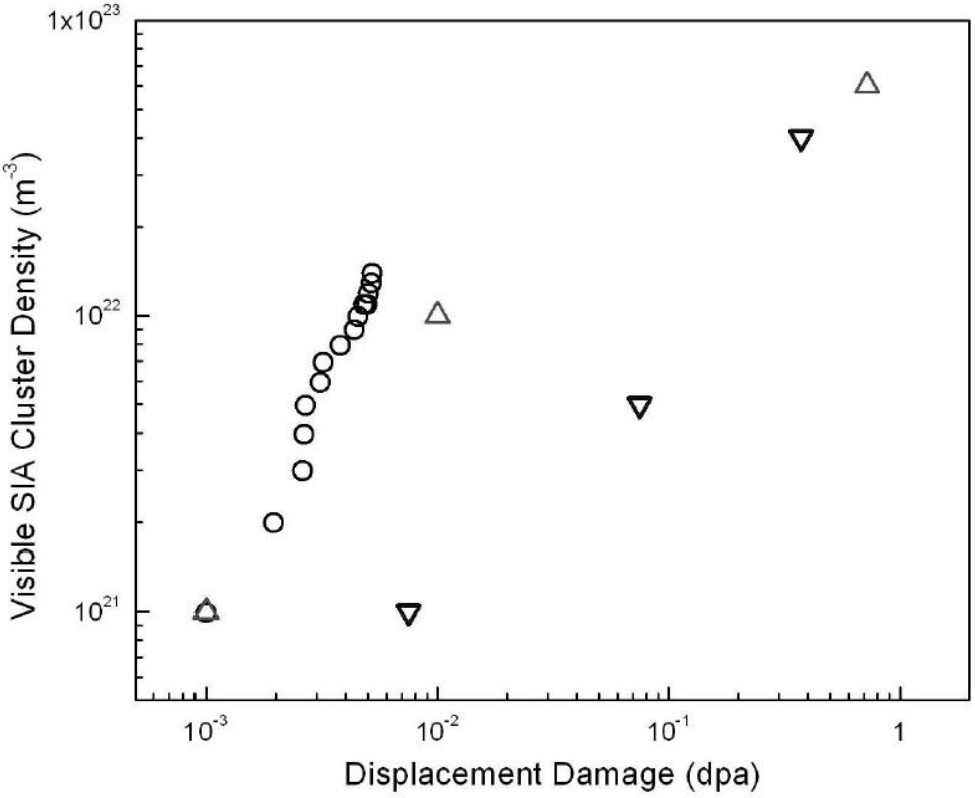

Figure 12. Dose dependence of visible SIA clusters density in bcc iron: (0) KMC simulation results, (Δ) and (∇) experimental results from references [7] and [33], respectively.

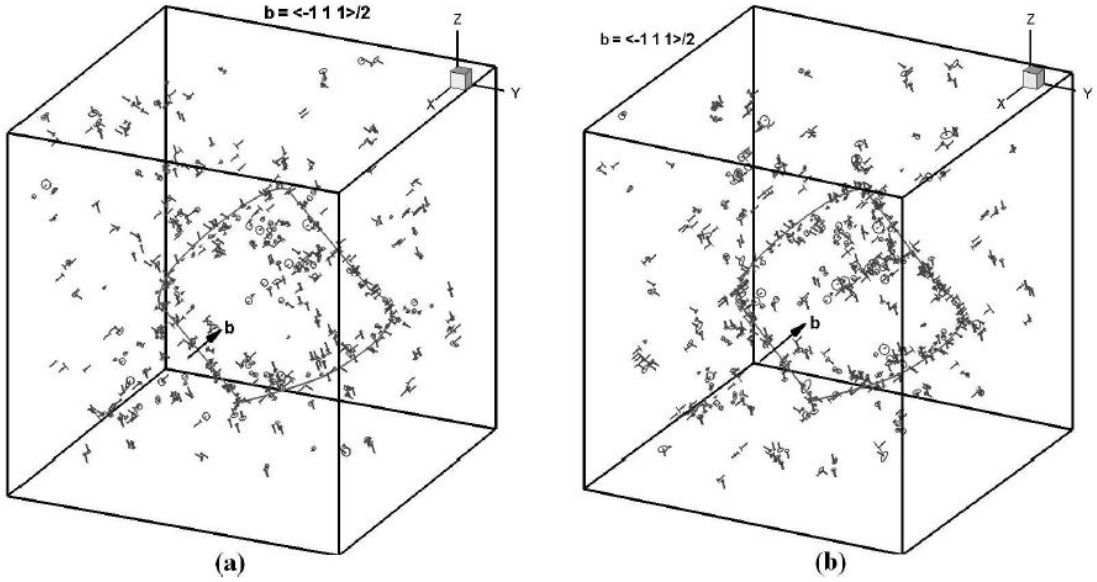

Figure 13. Dose dependence of dislocation decoration by SIA clusters produced in cascades at 300 K (a) at 1.3 x 10^{-3} dpa and (b) 5.2 x 10^{-3} dpa.

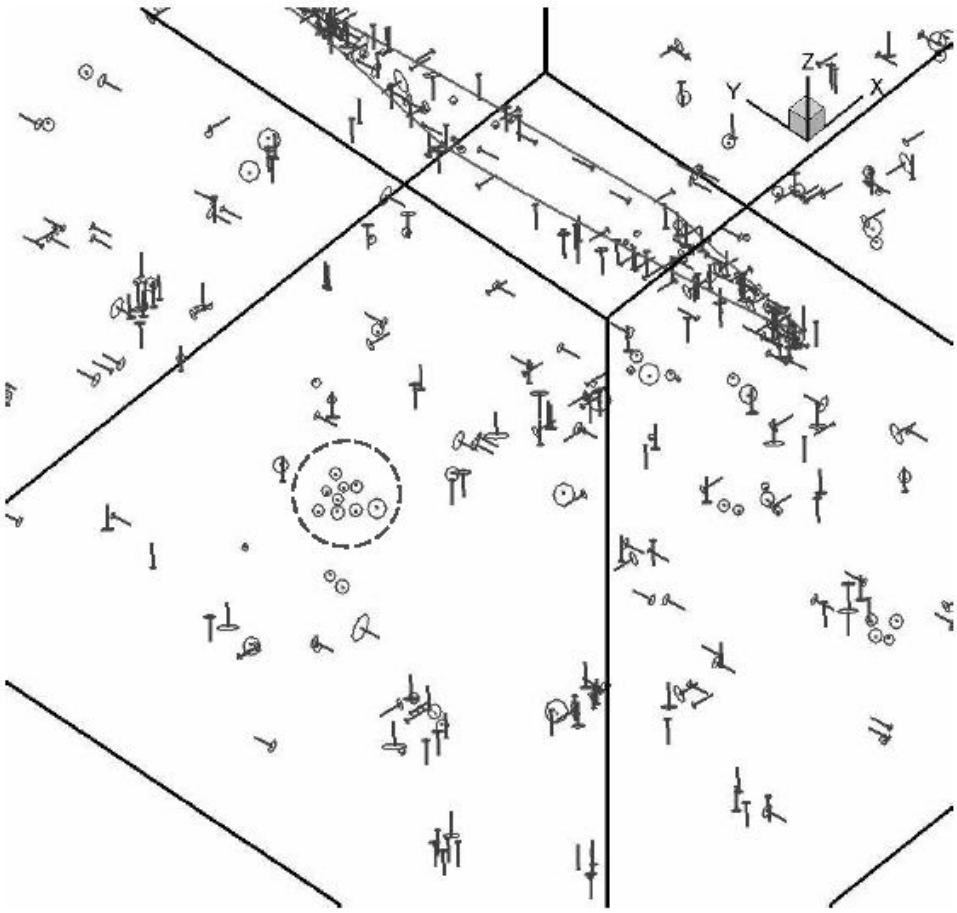

Figure 14. A close-up view of the configuration of a raft of SIA clusters formed at a dose level of 1.8×10^{-3} dpa: the raft is enclosed in a dotted circle.

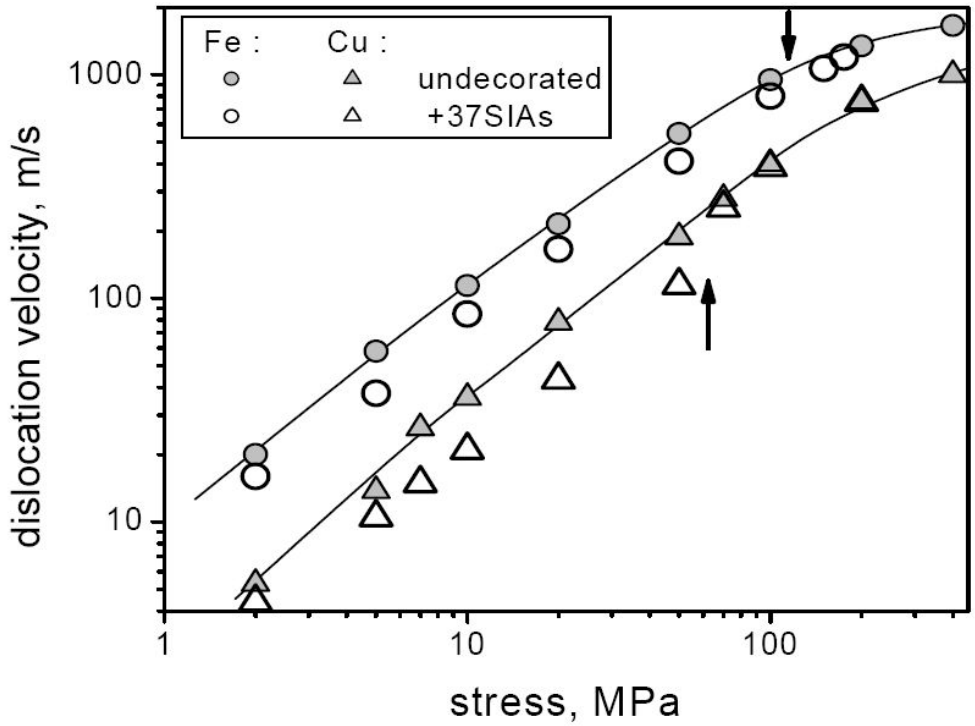

Figure 15. Dependence of dislocation velocity on applied resolved shear stress for undecorated (grey symbols) and decorated (open symbols) dislocations in iron (circles) and copper (triangles) simulated at 300 K. Vertical arrows indicate the stress at which the dislocation leaves the row of loops in the decoration.

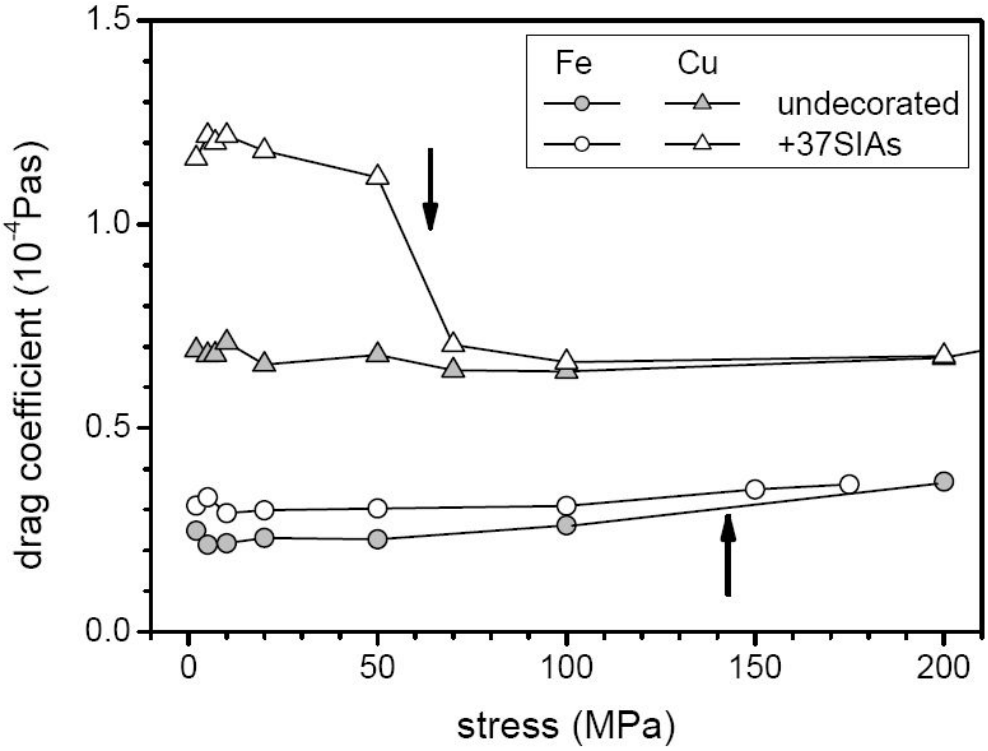

Figure 16. Drag coefficient versus applied resolved shear stress for undecorated (grey symbols) and decorated (open symbols) dislocations in iron (circles) and copper (triangles) simulated at 300 K. Vertical arrows indicate the level of breakaway stress at which the dislocation leaves the row of loops in the decoration.

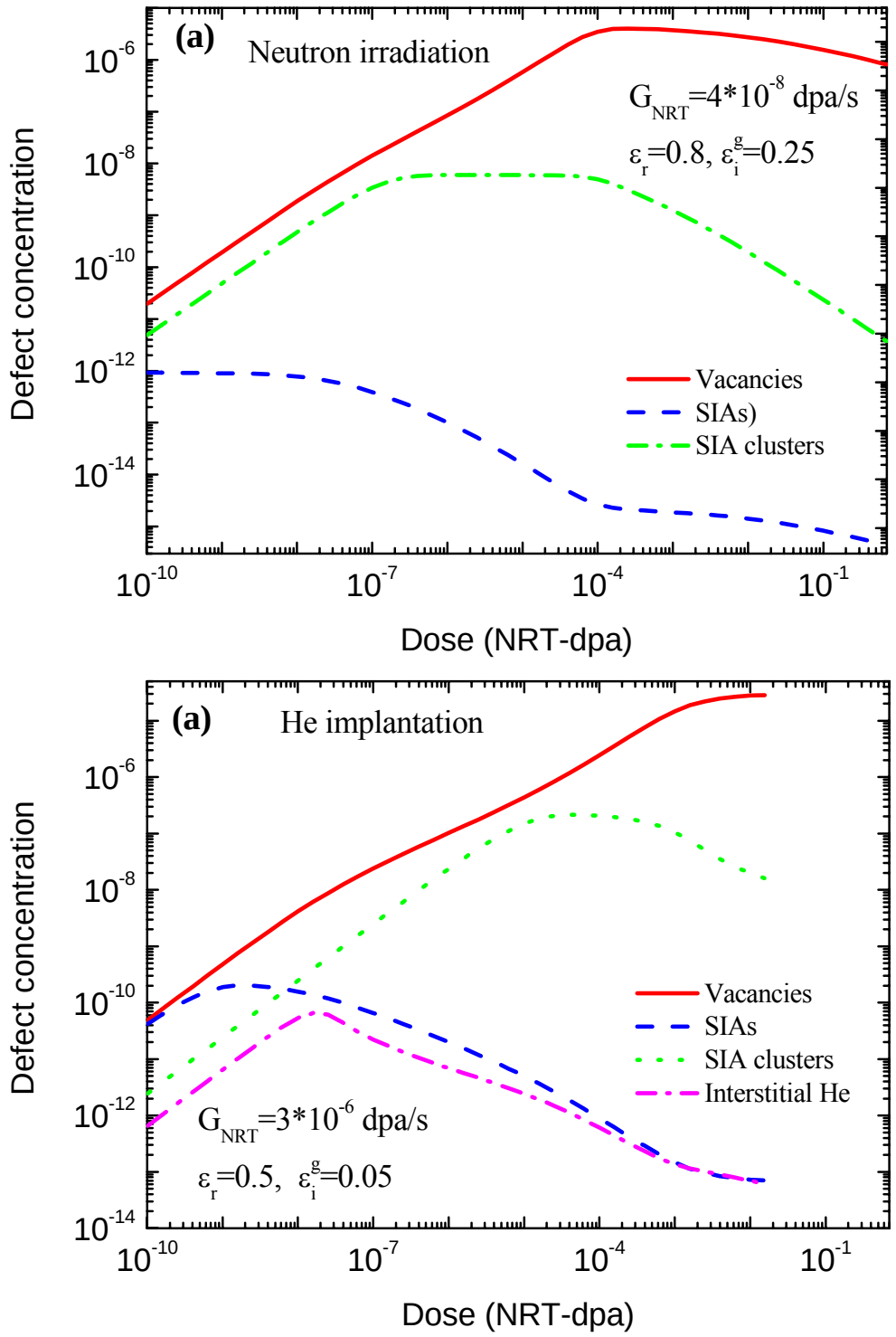

Figure 17. Dose dependence of density of mobile defects under (a) neutron irradiation and (b) helium implantation at 323 K calculated for a dislocation density of 10^{13} m^{-2} and a displacement damage rate of 4 x 10^{-8} dpa/s and 3 x 10^{-6} dpa/s, respectively. Note that in the case of neutron irradiation the vacancy concentration reaches its maximum already at a dose level of about 10^{-4} dpa whereas in the case of helium implantation the vacancy concentration does not reach a maximum even at a dose level of about 10^{-2} dpa.

Mission

To promote an innovative and environmentally sustainable technological development within the areas of energy, industrial technology and bioproduction through research, innovation and advisory services.

Vision

Risø's research **shall extend the boundaries** for the understanding of nature's processes and interactions right down to the molecular nanoscale.

The results obtained shall **set new trends** for the development of sustainable technologies within the fields of energy, industrial technology and biotechnology.

The efforts made **shall benefit** Danish society and lead to the development of new multi-billion industries.